Monitoring long-term forest dynamics with scarce data: a multi-date classification implementation in the Ecuadorian Amazon

Fabián Santos, Pablo Meneses & Patrick Hostert

Published online: 15 Oct 2018.

Submit your article to this journal ☑

Article views: 498

View Crossmark data ☑

Taylor & Francis
Taylor & Francis Group

Monitoring long-term forest dynamics with scarce data: a multi-date classification implementation in the Ecuadorian Amazon

Fabián Santos [a,b], Pablo Meneses[c] and Patrick Hostert [d,e]

aCenter for Remote Sensing of Land Surfaces (ZFL), University of Bonn, Bonn, Germany; bCenter for Development Research (ZEF), University of Bonn, Bonn, Germany; cObservatorio Científico, Universidad Regional Amazónica Ikiam, Tena, Ecuador; dGeography Department, Humboldt-Universität zu Berlin, Berlin, Germany; eIRI THESys – Integrative Research Institute on Transformations of Human-Environment Systems, Humboldt-Universität zu Berlin, Berlin, Germany

ABSTRACT

Monitoring long-term forest dynamics is essential for assessing human-induced land-cover changes, and related studies are often based on the multi-decadal Landsat archive. However, in areas such as the Tropical Andes, scarce data and the resulting poor signal-to-noise ratio in time series data render the implementation of automated time-series analysis algorithms difficult. The aim of this research was to investigate a novel approach that combines image compositing, multi-sensor data fusion, and postclassification change detection that is applicable in data-scarce regions of the Tropical Andes, exemplified for a case study in Ecuador. We derived biennial deforestation and reforestation patterns for the period from 1992 to 2014, achieving accuracies of 82 ± 3% for deforestation and 71 ± 3% for reforestation mapping. Our research demonstrated that an adapted methodology allowed us to derive the forest dynamics from the Landsat time series, despite the abundant regional data gaps in the archive, namely across the Tropical Andes. This study, therefore, presented a novel methodology in support of monitoring long-term forest dynamics in areas with limited historical data availability.

Introduction

The Amazon rainforest constitutes one of the biologically most diverse, structurally complex, and carbon-rich bioregions of the world (Asner et al., 2014). It performs essential global-scale functions and provides a multitude of ecosystem services (Paula et al., 2014). Tropical deforestation is a major threat to the region and a driver of climate change with potentially critical impacts on the biosphere (Fearnside, 2005). Large-area deforestation assessments indicate that the Amazon Basin lost 13.3% of its forest from 2000 to 2013, where the headwater basins suffered most of the pressure (RAISG, 2015). This is also particularly alarming for the region itself, as the highland Amazon (or Tropical Andes) is highly susceptible to global warming (Karmalkar, Bradley, & Diaz, 2008), while being under-researched in deforestation studies (Armenteras, Rodríguez, Retana, & Morales, 2011). Moreover, only little is known about forest succession (Barbosa, Broadbent, & Bitencourt, 2014) or land-cover intensities (Kuemmerle et al., 2013) in this subregion, which are also important components for understanding the impacts on ecological services (e.g. on biodiversity, carbon sequestration, or nutrient sinks; Brown & Lugo, 1990; Edwards, Massam, Haugaasen, & Gilroy, 2017; Poorter et al., 2016). Monitoring forest dynamics in the

Tropical Andes, therefore, plays a key role for informing policymakers and resource managers in their decision-making processes over the next few years (Angelsen & Wertz-Kanounnikoff, 2008; De Koning et al., 2011). While lowland tropical forests have been well researched, closing the remaining knowledge gaps on forest dynamics in Andean tropical forests is of prime importance (Armenteras, María, Rodríguez, & Retana, 2017; Da Ponte et al., 2015; Oliveira, Eller, Bittencourt, & Mulligan, 2014; Spracklen & Righelato, 2014).

Comprehensive forest dynamics monitoring has traditionally implied decades of field observations (Fragal, Silva, & Novo, 2016). Such observations are costly, and it might even be impossible to collect the necessary data in the field. Remote sensing offers a unique alternative for supplying this information for large areas and in different spectral, spatial, and temporal resolutions. Terra and Aqua on board of the Moderate Resolution Imager Spectroradiometer (MODIS) have regularly been used for broad-scale mapping of forest dynamics (Hansen et al., 2008). However, the spatial resolution of MODIS data is limited when fine-scale disturbance regimes prevail such as from selective logging, skid trails, or disturbances related to landslides or local windthrow. The Landsat sensor family with its 30-m spatial resolution

---

This article has been republished with minor changes. These changes do not impact the academic content of the article.

and its 45-year observation record is better suited for capturing long-term and fine-scale processes. It is the most widely used observation system for land-cover and land-use change (LCLUC) assessments and forest dynamics monitoring programs (Camara, 2013; Hansen & Loveland, 2012). Since the launch of Landsat-1 in 1972, the Landsat Program has continuously collected data across the globe and – since the launch of the Landsat Thematic Mapper (TM) in 1982 – in six spectral bands covering the optical, near-infrared, and shortwave infrared wavelength regions. For these reasons, it is the most long-term medium-resolution Earth observation satellite archive available. Due to the open data policy since 2008, Landsat data are available free of charge as a standard high-level product for long-term LCLUC analysis (Wulder et al., 2016). This development allowed major improvements in automated time-series analysis, leading to a range of novel algorithms such as TIMESAT, LandTrendr, BFAST, and CCDC (Eklundh & Jönsson, 2015; Kennedy, Yang, & Cohen, 2010; Verbesselt, Hyndman, Newnham, & Culvenor, 2010; Zhu & Woodcock, 2014) that allow for extracting forest dynamics information. However, in some regions around the globe, the archive data density is considerably lower, mostly due to persistent cloudiness (Arvidson, Gasch, & Goward, 2001; Chance, Hermosilla, Coops, Wulder, & White, 2016) reduce data quantity and quality. This results in time series with poor signal-to-noise ratio, as useful information about forest status is weak and not significant to differentiate from random noise. This is a limitation for transferring these novel algorithms to data-scarce regions, such as the Tropical Andes (Santos, Dubovyk, & Menz, 2017), as time series analyses require rather dense data stacks over time.

Conceptual approaches including those based on image compositing, multi-sensor fusion, and postclassification change detection have demonstrated their potential to overcome these limitations (Griffiths et al., 2014; Hansen et al., 2013; Potapov et al., 2012). Multi-date classification (Zhu, 2017) has the advantage to cope with noise-prone observations, especially when based on cloud-free composites that not only allow identifying deforestation or reforestation processes but also to characterize land-use intensities from post-deforestation dynamics (Rufin, Müller, Pflugmacher, & Hostert, 2015). For these reasons, multi-date classification is the methodology of choice for monitoring long-term forest dynamics in areas such as the Tropical Andes. However, implementing a multi-date classification scheme under specific regional conditions can still be challenging, for example, due to poor data availability in the past depending on historical data receiving strategies or increased cloudiness due to topography. Consequently, we applied this methodology to a study case located in the Amazon region of Ecuador, the Upper Napo Watershed (UNW), where heavy rainfall regimes (Espinoza et al., 2015) and complex landscapes (Asner et al., 2014) are major impediments. Our overarching objective was to monitor long-term forest dynamics and identify deforestation/ reforestation for the period between 1992 and 2014. We pose the following research questions related to these objectives:

- Which processing steps and techniques are needed to implement multi-date classification in a data sparse region, as exemplified in the UNW?
- How well does a multi-date classification approach perform when monitoring long-term forest dynamics in the environments of the Tropical Andes?

Study area

The UNW is located between 78°25′W and 76°25′W longitude and 0°10′N and 1°30′S latitude (Figure 1 (a)). It covers an area of about 12,500 km^2 in the Ecuadorian Amazon, spreading across the three provinces Napo (63% of the watershed), Orellana (26%), and Pastaza (9%). The altitudinal gradient of the Andes covers ~260–5600 m above sea level (a.s.l.). Mean temperatures varying from −0°C to 26°C and annual precipitation from 1100 to 5300 mm (MAE, 2013). The core rainy season extends from December to May, but fog and clouds are abundant throughout the year, especially at higher elevations (Ramírez, Teuling, Ganzeveld, Hegger, & Leemans, 2017). The complex geology creates diverse edaphic conditions that in combination with topographic gradients and climatological impacts results in a multitude of extremely species-rich ecosystems (Hoorn et al., 2010).

The percentage of natural vegetation in the UNW was estimated to be 79% in 2014, with 76% of forest, 2% of shrub-dominated landscapes, and 1 % of grasslands (MAE, 2017). Forests are generally evergreen, but forest ecosystems vary substantially in tree composition, flood regimes, and topographic and bioclimatic boundary conditions (MAE, 2013). According to Guariguata and Ostertag (2001), reforestation occurs as quickly as in 5 years after a disturbance in the evergreen forest ecosystems of the Ecuadorian Amazon, with variations depending on past land use practices and abiotic site conditions. This was verified during fieldwork in May 2017 at three reforestation sites in the UNW, where 46 hemispherical photographs were acquired. We followed Pueschel, Buddenbaum, and Hill (2012) to binarize these photographs and derive the canopy closure index. We found that canopy closure after 5 years can be greater than of a 20-year-old forest (Figure 1(b)). We accordingly used a time threshold of 5 years as a

(a)

(b)
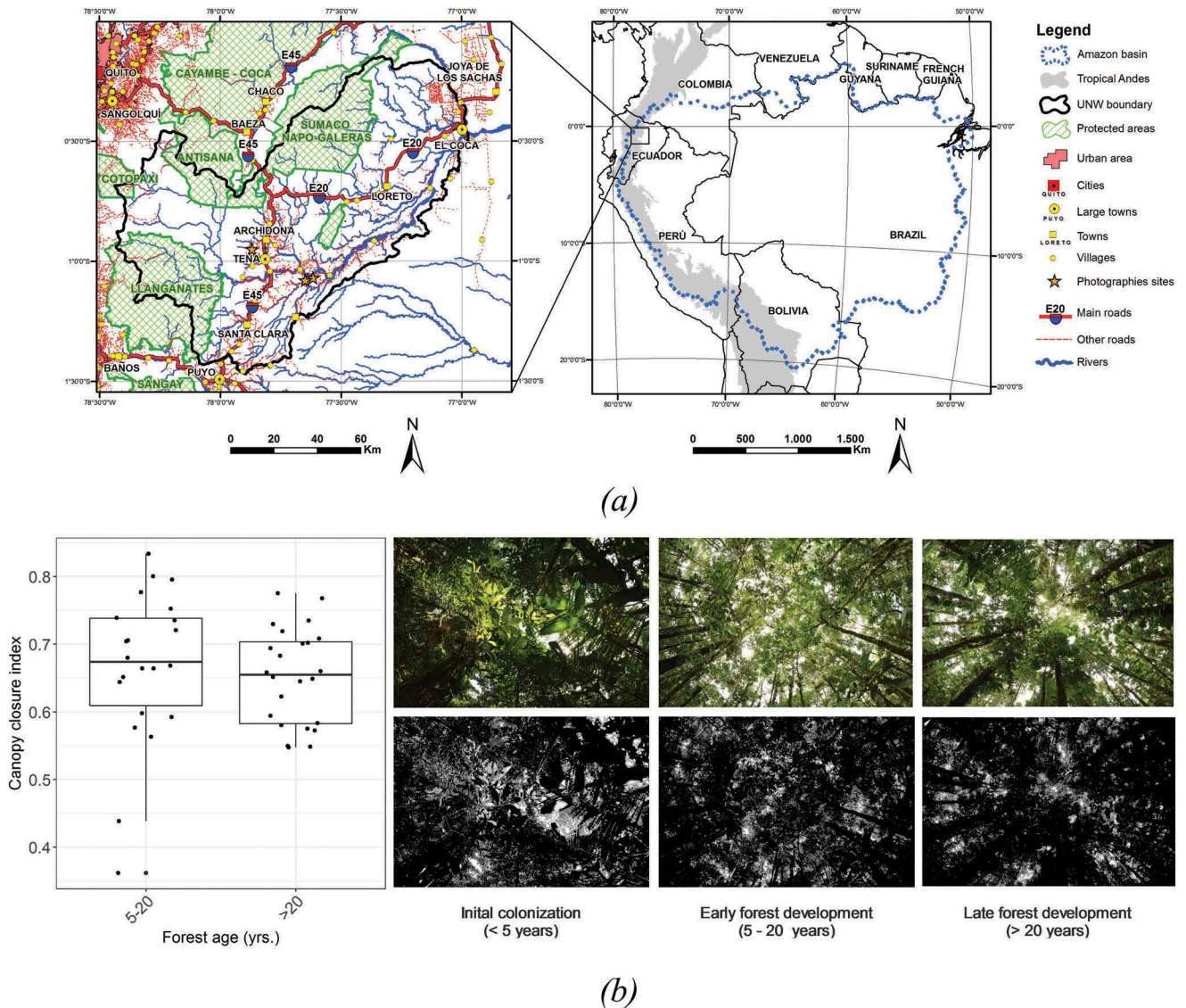
Figure 1. (a) The UNW study area, localization in the context of the Amazon Basin and the Tropical Andes. (b) Boxplot of the canopy closure index and estimated forest age and hemispherical photographs with derived canopy closure index for different forest development stages.

reference for mapping reforestation (compare "Materials and methods" section). Four National Protected Areas, mainly created during the 1990s, are present in the UNW and cover 25% of the total area. 78,300 ha of native forest were reported to be converted to pastures and croplands between 2000 and 2014, resulting in an average annual deforestation rate of ~6300 ha or 0.5% of the forested land (MAE, 2017). While these numbers vary, deforestation rates do not exceed 1.2–1.6% yr^{-1} (Sierra, 2000).

Materials and methods

We organized the processing in five main steps (Figure 2) when implementing our multi-date classification. All procedures were developed in the R language (R Development Core Team, 2017), and different strategies were applied to improve the

processing (e.g. parallelization, vectorization, and c-code libraries; Bengtsson, 2016; Clayden, 2016; GDAL Development Team, 2017; Hijmans, 2016; Weston, 2015) in complex computations.

Data and preprocessing

For this study, we downloaded 1350 images for four Landsat footprints (09–60, 09–61, 10–60, and 10–61) and for the period 1989–2016. They were processed to surface reflectance and acquired from the United States Geological Survey (USGS) Global Archive, sourced through the Earth Resources Observation and Science (EROS) Center Science Processing Architecture (ESPA; USGS, 2014). This data-set included Landsat TM, Enhanced Thematic Mapper plus (ETM+), and the Operational Imager (OLI) data. This ready-to-use data-set is radiometrically
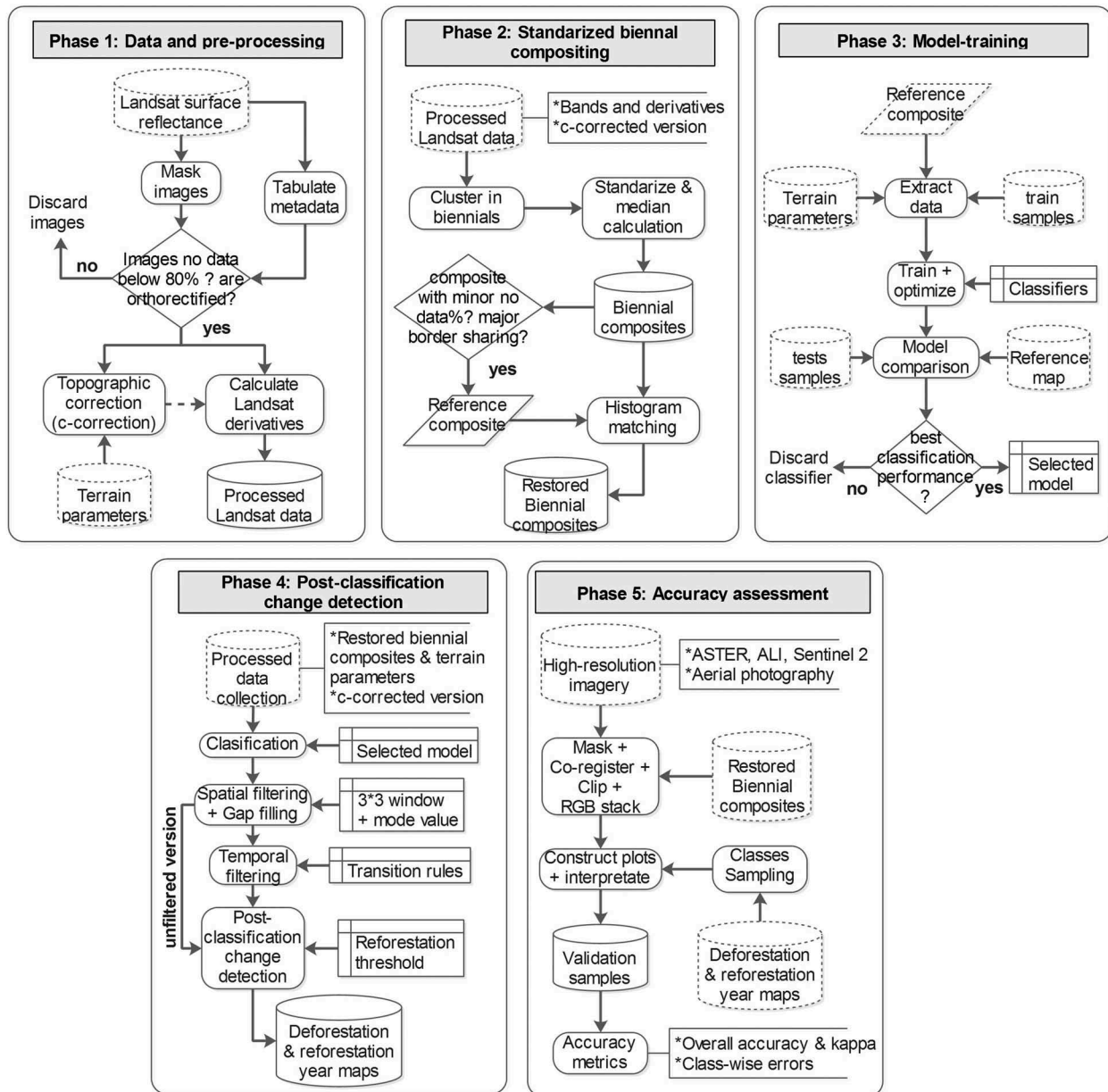
Figure 2. Methods and workflow for implementing the multi-date classification.

calibrated by the Landsat Ecosystem Disturbance Adaptive Processing System (LEDAPS; Masek et al., 2012) and orthorectified using a digital elevation model (DEM) and ground control points (NASA, 2011). The percentage of masked areas (or no-data pixels) for each image was calculated using C code based on the Function of Mask (Fmask) algorithm (CFmask; Zhu & Woodcock, 2012) and LEDAPS by merging cloud, cloud shadow, glacier, and water areas into a unique class (Figure 3(a)). Images with percentages above 90% of no-data pixels and images without orthorectification according to their metadata were omitted, reducing the time series of 27 years to effectively 23 years since 1991 (Section "Postclassification change detection"). In total, 288 images were used (i.e. 68, 79, 74, and 67 images per Landsat footprint, respectively) to complete the multitemporal composites. Data were mostly available during the dry season

(67% of images, Figure 3(b)), while the fewer images acquired during the rainy season avoid additional data gaps in single years for our forest dynamics analyses (Kimes, Nelson, Skole, & Salas, 1998; Lunetta, Johnson, Lyon, & Crotwell, 2004). This is in contrast to other studies, which selected images from specific periods within a year (Müller, Griffiths, & Hostert, 2016). However, we preferred to maintain all images as a strategy to reduce data loss in this data-sparse environment. The average time interval between consecutive images for each footprint was 141, 122, 130, and 154 days, respectively. Nevertheless, in all footprints, a data gap from August 1992 to July 1996 in the Landsat archive, introduced an interruption of 3.9 years in our time series. Finally, a set of vegetation indices, band ratios, and Tasseled Cap transformation derivatives were calculated from the Landsat images (Table 1) following recommendations from similar
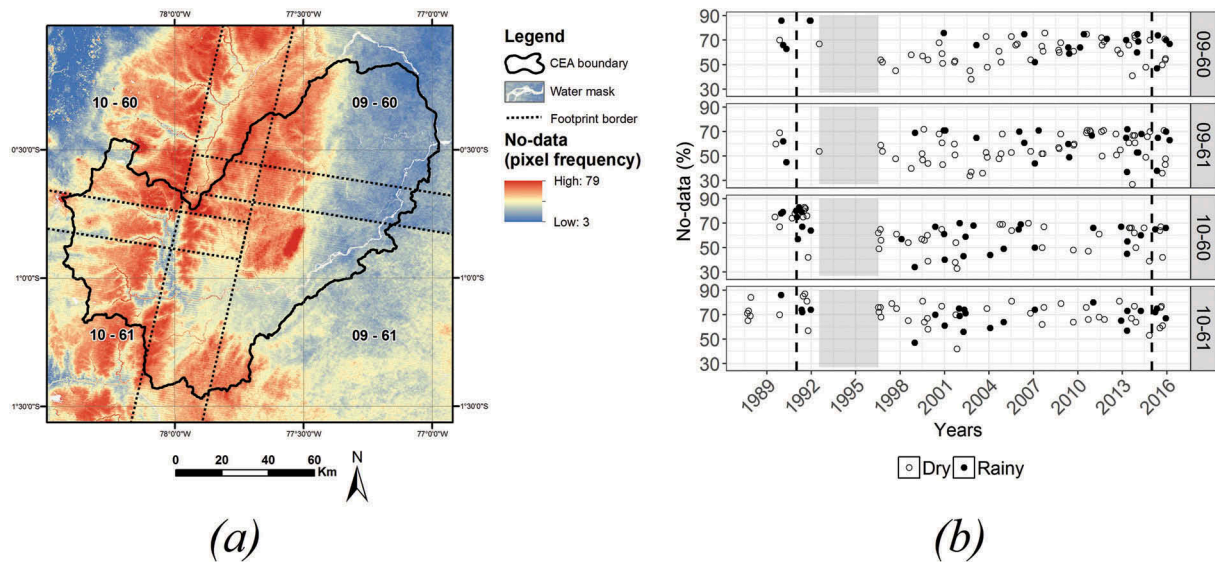
Figure 3. (a) Spatial distribution of no-data pixel frequencies and (b) no-data percentage of selected images. Gray areas in the plots refer to the 1992–1996 data gap and dashed lines to effective 23 years' time series.

Table 1. Landsat bands and derivatives.

Name	Abbreviation	Wavelength region	References
Normalized Difference Vegetation Index	NDVI	VIS, NIR	Rouse, Haas, Scheel, and Deering (1974)
Aerosol Free Vegetation Index 1.6-μm band	AFRI16	NIR	Karnieli, Kaufman, Remer, and Wald (2001)
Normalized burn ratio	NBR	NIR	Key and Benson (2006)
Landsat bands 1–7	Bands 1–7	VIS, NIR, SWIR	–
Band ratios: TM4/TM3, TM5/TM4, TM5/TM7	R43, R54, R57	VIS, NIR, SWIR	Krishna Bahadur (2009)
Tasseled cap: brightness, greenness, and wetness	TCB, TCG, TCW	VIS,NIR, SWIR	Crist and Cicone (1984)

forest dynamics studies (Kennedy et al., 2010; Müller et al., 2016; Potapov et al., 2012). To overcome the topographic effects, a c-correction algorithm (Riaño, Chuvieco, Salas, & Aguado, 2003) was applied to Landsat bands and its derivatives to evaluate whether it contributes to improving classification results (Section "Accuracy metrics results").

We collected 872 image chips from different sources acquired between April 2000 and August 2016 from high- and very high-resolution data for validating our medium-resolution remote sensing outputs (Olofsson et al., 2014): aerial photography (1-m spatial resolution), pan-sharpened images from the Advanced Land Imager (ALI, 10 m), Sentinel-2a (10 m), and Advanced Spaceborne Thermal Emission and Reflection Radiometer (ASTER) imagery (15 m). The latter is available for free (National Institute of Advanced Industrial Science and Technology & Geological Survey Japan, 2017), and we downloaded the whole archive to densify our high-resolution validation dataset. All images were preprocessed including manual co-registration (using Landsat imagery as a reference) and cloud masking including shadows (applying simple thresholds and manual screening in some cases). Finally, multispectral imagery were stacked, that is, ASTER, ALI, and Sentinel, for display them as false-color composites during the construction of validation samples plots (Section "Accuracy assessment").

To guide our implementation (Section "Postclassification change detection"), the information used for the establishment of Ecuador's Forest Reference (EFR) Emission Level (MAE, 2017) was collected. This data-set constitutes a series of land-cover and vegetation maps based on Landsat, ASTER, and Rapid Eye imagery that were visually interpreted with accuracies around 70% for different periods between 1990 and 2014.

For the elevation source, we used the three arc-second (90 m) DEM from the Shuttle Radar Topography Mission (SRTM; CGIAR – CSI, 2008). This data-set corrected for data gaps and its quality is, especially for mountainous regions of Ecuador, higher than the one arc-second (30 m) resolution product. We derived elevation, slope, aspect, roughness, the topographic position index (TPI), and the terrain ruggedness index (TRI; Wilson, O'Connell, Brown, Guinan, & Grehan, 2007) to evaluate their contribution to classification performance.

Standardized biennial compositing

For compositing, we discarded Landsat bands 1 and 2 as they are known to be more sensitive to atmospheric effects (Zhang, Carder, Muller-Karger, Lee, & Goldgof, 1999), while Landsat bands 3, 4, 5, and 7 and the calculated derivatives described in Table 1

were grouped in biennials according to the acquisition date of the image used in their calculation. The biannual time step was chosen as it resulted in 5 ± 2 images being available for most composite cases. This arrangement resulted in a no-data percentage average of 34 ± 13% (Figure 4(a)).

All biannual input pixels were z-transformed for the compositing:

$$Z_{ij} = \rho_{ij} - \mu_j/\sigma_j \qquad (1)$$

with ρ_{ij} being the pixel vector at position i and for date j, and μ and σ being the pixel's mean and standard deviation at date j. We then calculated the median $\bar{Z}_i$ value for each vector Z_i as this metric is known to be less affected by atmospheric contamination or phenological variation in image compositing (Potapov et al., 2012). Other metrics (e.g. quantiles, maximum, minimum, and variance) that are regularly applied in similar studies (De Fries, Hansen, Townshend, & Sohlberg, 1998) were also tested. However, the data-scarce situation required a conservative approach using the median. Finally, we normalized $\bar{Z}_i$ and stored it as the output value β for a given biennial composite according to

$$\beta = \frac{\bar{Z}_i - min(\bar{Z}_{i:n})}{max\ (\bar{Z}_{i:n}) - min(\bar{Z}_{i:n})} \qquad (2)$$

As residual radiometric offsets occur in the overlap areas between footprints, we required a pixel-level radiometric alignment (Pflugmacher, Cohen, & Kennedy, 2012). We selected the 2002 composite from path-row 09–60 and 09–61 as reference composites, as they had few no-data values and a low atmospheric aerosol load. Values in the overlapping footprints (10–60 and 10–61) were aligned based on histogram matching across the overlap areas to neighboring footprints. The same procedure was then applied across the time series within each footprint. In total, 52 biennial composites where aligned with references footprints, reducing, for example, the variance of the tasseled cap brightness (TCB) from 0.1 to 0.01 after histogram matching (Figure 4(b)).
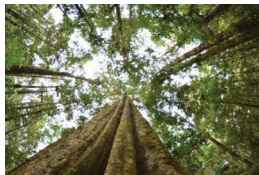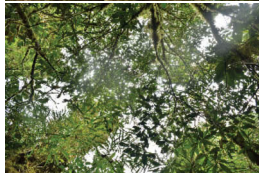
Model training

We defined four classes to map permanent forest cover and deforested/reforested areas. Permanent forests included, on one hand, evergreen forests (encompassing montane, foothill, lowland, and flooded forests) and, on the other hand, *Guadua* spp. forests with their spectrally distinct patterns due to their different species composition, canopy height, and overall lower biomass (Silman, Ancaya, & Brinson, 2003). Other nonforest"" vegetation above 3300 m a. s.l. such as grasslands or shrubs were not considered in this research. Conversely, change classes included human land use for agricultural production, that is, pastures and croplands (including early revegetation, commercial, and subsistence plantations), and nonvegetated areas, that is, bare soils and urban areas. We gained initial knowledge of the approximate class distribution by running a first and nonvalidated image classification with a few training samples, which built the basis for distributing the training samples for training in a guided fashion (Table 2).

We then interpreted the almost 1000 training samples on-screen based on a mosaicked, biennial color composite from 2002 and on a recent vegetation map (MAE, 2017). Since the four classes represented a complex spectral feature space and their visual separation was challenging (Figure 5(a)), we tested different classifiers using the caret package (Kuhn, 2016). This software applies a parameter tuning of classifiers and bootstraps training samples
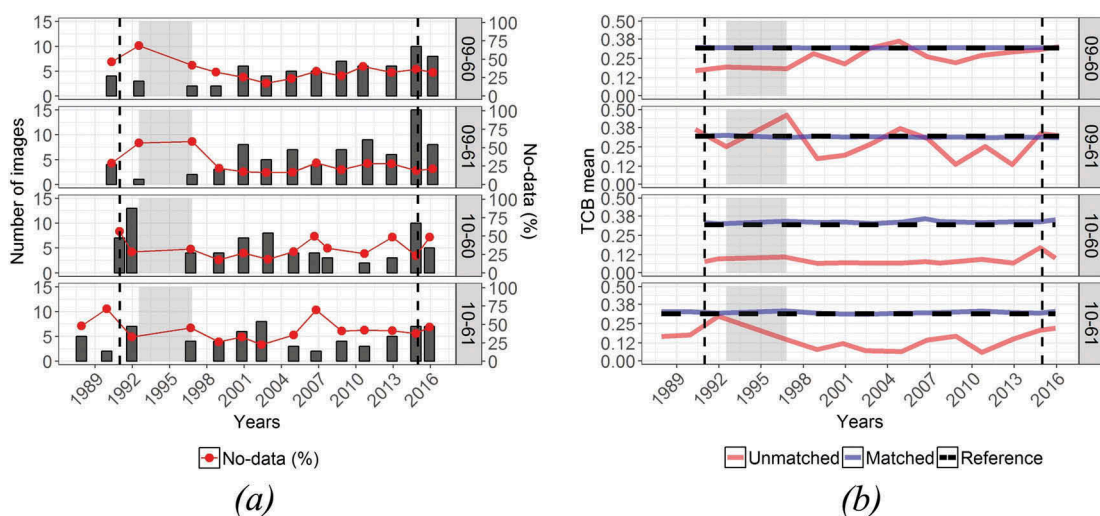

Figure 4. (a) Number of images used for compositing and no-data percentage in resulting composites and (b) tasseled cap wetness (TCW) mean value of composites with (matched) and without histogram matching (raw). Gray areas in the plots refer to the 1992–1996 data gap and dashed lines to effective 23 years' time series.

Table 2. Classes considered and training sample size.

Type	Classes	Approximate area (km²)	Samples (no.)	Example photograph
Permanent classes	Evergreen forest	8053	307	
	Guadua spp. forest	181	122	
Change classes	Pastures/croplands	2047	279	
	Bare soil/urban areas	653	221	

A class-wise standard deviation of 0.9 and a confidence interval of 0.9 were considered to obtain a reasonable class-wise sample size.
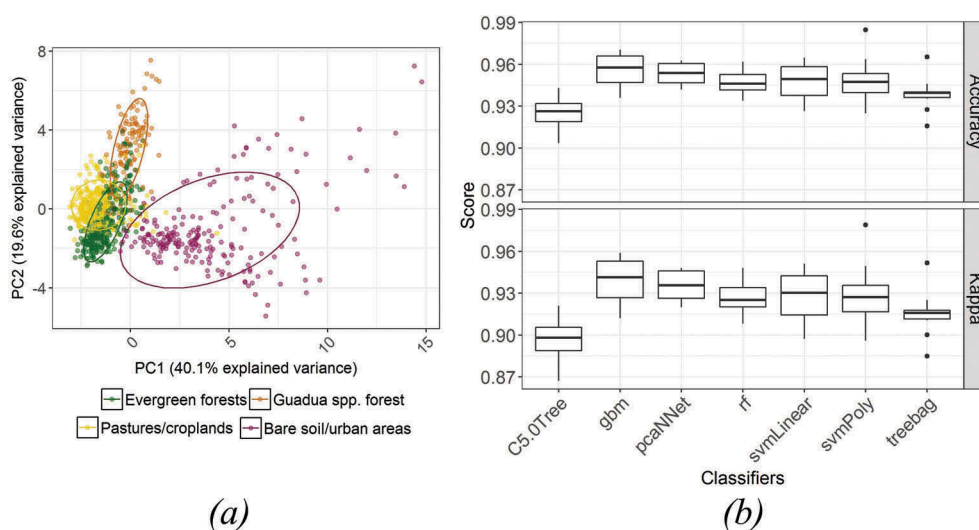
Figure 5. (a) The feature space of the training samples using the first and second principal components (PC1 and PC2) obtained from Landsat bands, derivatives, and terrain parameters. (b) Boxplots of classifiers' out-of-bag error using training samples.

to determine their effect on performance and decided on an optimal model. As most classifiers provided similar out-of-bag error (Figure 5(b)), we decided to use a least squares support vector machine (SVM) with polynomial kernel (svmPoly; Karatzoglou, Smola, Hornik, & Zeileis, 2004), as it achieved the highest overall correlation (0.697) with the land-cover reference maps (MAE, 2017). Other classifiers including Random Forest (rf, 0.684), Stochastic Gradient Boosting (gbm, 0.682) or Neural Networks (pcaNNet, 0.680) showed good correlations, but they were not higher than svmPoly.

Postclassification change detection

By classifying biennial composites, 13 land-cover maps were obtained for each footprint, covering the period 1989–2016. A 3 × 3 median filter was applied to eliminate spurious pixels within a land-cover map, but for data gaps, values were input calculating the per-pixel time-series mode from all land-cover maps. While random noise and discontinuities were eliminated, artifacts from clouds and cloud shadow remnants, sensor noise, or simply misclassified pixels were still present in the data. Therefore, we further applied a temporal filter with transition rules (Clark, Aide, Grau,

& Riner, 2010) to identify illogical land cover and land-cover change patterns and reclassified errors according to a set of rules based on contextual knowledge. For example, it is impossible that bare soil becomes an evergreen forest in 1 year and returns to the bare soil class the next year again. Instead, this may represent either cropped land (bare soil or cropped land in 1 year) in the case of agricultural land, or it simply may be a misclassification. In any case, it will not represent land change associated with forest cover. We accordingly implemented a temporal filter based on a moving window of three consecutive observations and a set of allowed transition rules (Table 3).

Since the first and the last land-cover maps could not be temporally filtered according to this scheme, we omitted those years (i.e. 1989–1991 and 2015–2016 periods), thereby reducing our time series to the period 1992–2014, that is, 11 observations for each footprint.

We then derived deforestation and reforestation dates from the series of land-cover maps. We flagged the first year of a forest pixel being mapped as one of the nonforest classes as the deforestation year. Reforestation, though, is a continuous process that can only be mapped from satellite data once a certain threshold of "forestedness" has transgressed, that is, a previously nonforested pixel spectrally resembles a forest class for a minimum period of time (defined in this article in 5 years as described in Section "Study area").

Finally, the outputs of the postclassification change detection were mosaicked and the UNW area extracted, considering the treeline (3300 m a.s.l.) to exclude nonforested areas. As our aim was to evaluate different algorithms for multi-date forest change classification, we iterated all these steps for each preprocessing approach (i.e. surface reflectance or topographic correction) and omitted/applied temporal filtering to evaluate their individual contribution to the overall accuracies of these maps.

Accuracy assessment

We calculated confusion error matrices for deforestation and reforestation maps (Cohen et al., 2017; Olofsson et al., 2014; Thomas et al., 2011). We employed a stratified random sampling based on the deforestation and reforestation classes, arranging samples of 5–3 pixels in a cross shape (Figure 6(a)). We sampled a minimum of 50 samples per class and

100 for the larger classes of stable forest and stable nonforest. Since reforestation stable classes could be affected during postclassification change detection due to its assigned regrowth-time threshold, we sampled these classes independently to ensure their performance. Finally, as spatial autocorrelation can bias the accuracy assessment (Congalton, 1991), a minimum threshold distance between samples of the same class was applied (Table 4).

Each sample was interpreted on-screen based on high-resolution imagery (Figure 6(b)) and Landsat color composites (Figure 6(c,d)). We calculated the overall accuracy, the kappa index, and class-wise commission and omission errors.

Results

Variable importance and svmPoly optimization report

We decomposed the svmPoly model to observe which variables contributed to the respective results. Figure 7(a) reveals that Landsat bands 4–7 and TCB, TCW, and tasseled cap greenness (TCG) yielded an importance above 90% in all classes. Conversely, vegetation indices and band ratios as well as terrain parameters were overall less significant but contributed to separating pastures/croplands from the *Guadua* spp. forests. These overlapped spectrally, but separability improved when integrating terrain derivatives in the classification process. Regarding optimization, the caret software explored three parameters of the svmPoly classifier (degree, scale, and cost) to maximize its classification accuracy (Figure 7(b)). Its final calibration yielded 274 support vectors with a cost of constraints (C) of 1, and the hyperparameter values were set to a degree of 3, scale of 0.001, and a default offset of 1.

Accuracy metrics results

Deforestation and reforestation maps based on different filtering techniques varied substantially (Table 5).

Overall accuracies were significantly better when applying surface reflectance and temporal filtering to land-cover classifications, achieving 82 ± 3% and 71 ± 3% (calculated with a 95% confidence interval) for deforestation and reforestation maps, respectively. Topographic correction led to poorer overall accuracies by 13 ± 2% in both maps when compared to the

Table 3. Transition rules.

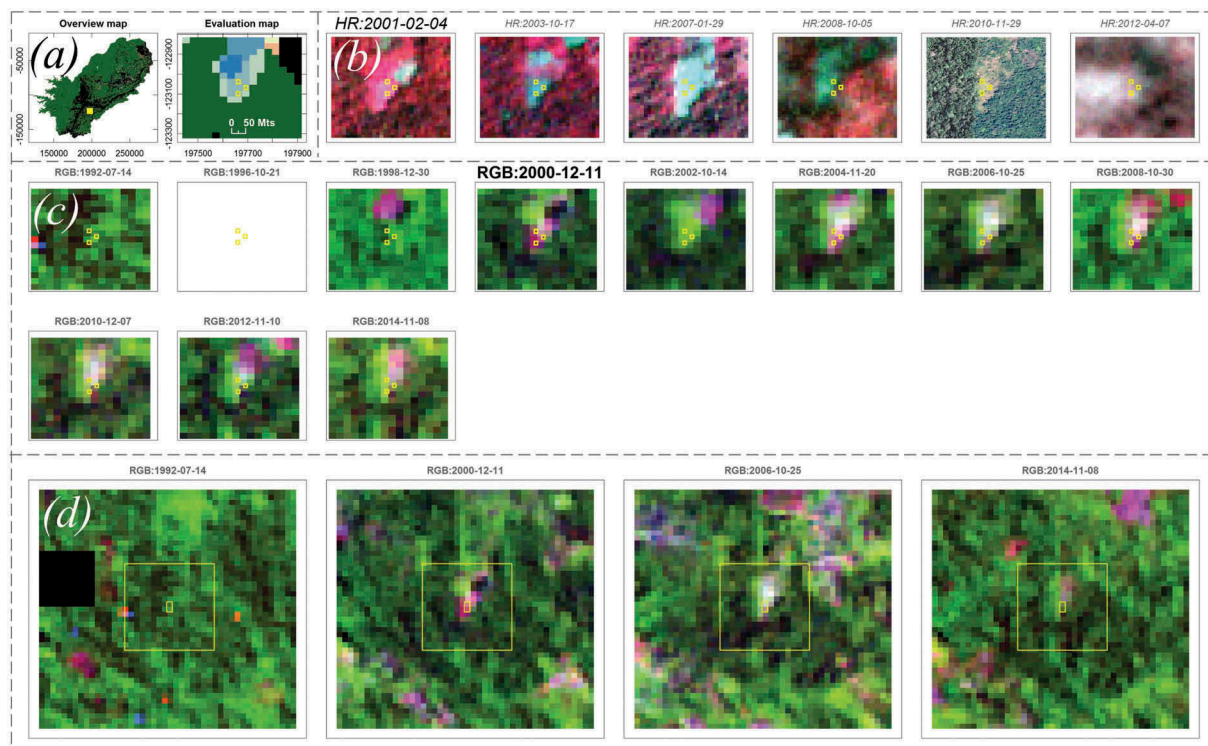|	Classes	Year $n + 1$			
		Evergreen forest	*Guadua* spp. forest	Pastures/croplands	Bare soil/urban areas
Years n and $n + 2$	Evergreen forest	Yes	No	No	No
	Guadua spp. forest	No	Yes	No	No
	Pastures/croplands	No	No	Yes	Yes
	Bare soil/urban areas	No	No	Yes	Yes

Figure 6. Example of a forest-loss sample (3 pixels). (a) Location of the sample in the map. (b) High-resolution image chips from ASTER (2001–2008 and 2012) and aerial color photography (2010). (c) Landsat color composites image chips (1992–2014, with a data gap in 1996) and (d) overview of them, showing the sample area and analysis period.

Table 4. Classes, minimum distances, and sample sizes.

Map	Class name	Distance threshold (m)	Sample size (pixel)
Deforestation map	Stable forest	2500	100
	Stable nonforest	2500	100
	Deforestation year	2500	50/year
Reforestation map	Stable forest	2500	100
	Stable nonforest	2000	100
	Reforestation year	1500–2000	50/year
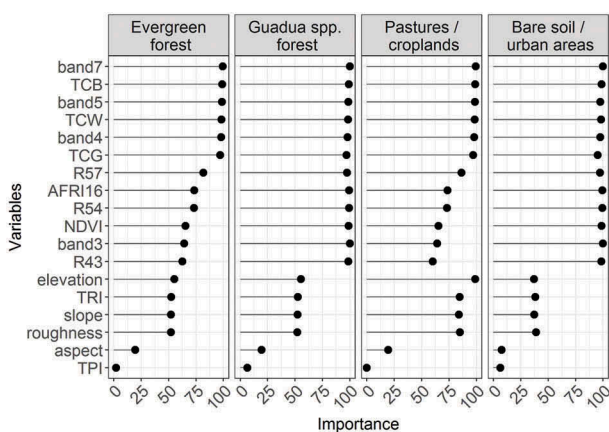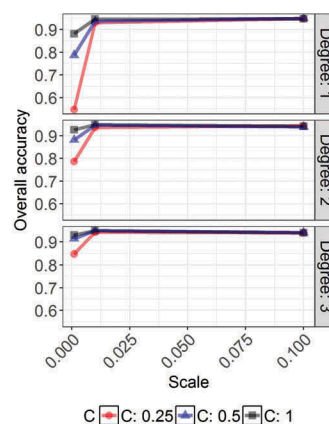
Figure 7. (a) Variable importance by class during classification with svmPoly. (b) Optimization of the svmPoly classifier during the model-training phase.

Table 5. Overall accuracy of deforestation and reforestation maps by processing approaches.

		Processing approaches		
Map	Accuracy metrics	Surface reflectance – not filtered (%)	Topographic correction – filtered (%)	Surface reflectance – filtered (%)
Deforestation	Overall	62	70	82
	Kappa	58	65	80
Reforestation	Overall	48	56	71
	Kappa	39	47	67

best result. Temporal filtering improved accuracies substantially by 21 ± 1% for both deforestation and reforestation maps. Commission and omission errors for stable and change classes are shown for the filtered product (Table 6).

The overall commission and omission errors were lower for the deforestation map (mean of 19% and 5%, respectively) than reforestation map (mean 32% and 11%, respectively). Moreover, stable classes were less prone to commission and omission errors (mean 1–11%) compared to change classes (mean 0–46%).

Deforestation and reforestation maps

Maps of deforestation and reforestation years are shown in Figures 8(a) and 9(a). In general, the patterns follow the description of Wasserstrom and Southgate (2013) for the Ecuadorian Amazon during its oil-related colonization (1964–1994). For instance, deforested areas along the E45 highway (built in 1975) and

the banks of the Napo River relate to settlements that already existed before the period we analyzed. The age of the deforestation patches along the E20 highway (built in 1983) decreased with increasing distance from the highway (Figure 8(b-1)). In the mountainous areas, the detection of landslide scars (Figure 8(b-2)) was accurate, and topographic shadows did not apparently inhibit the change detection. However, false-positive errors were observed not only in areas with many mixed pixels where mostly evergreen forests and pasture/cropland occurred (Figure 8(b-3)) but also in areas with no-data values due to the occurrence of sparse observations or an inaccurate water mask.

Areas of reforestation seemed to be more prominent along the E45 highway, where deforestation was less intense. Known areas of reforestation since the 1990s were well represented (Figure 9(b-1)), as was forest succession after landslides in mountainous areas (Figure 9(b-2)). Overall, the reforestation year map was more affected by mixed pixel problems and

Table 6. Commission and omission errors for the surface reflectance – filtered approach.

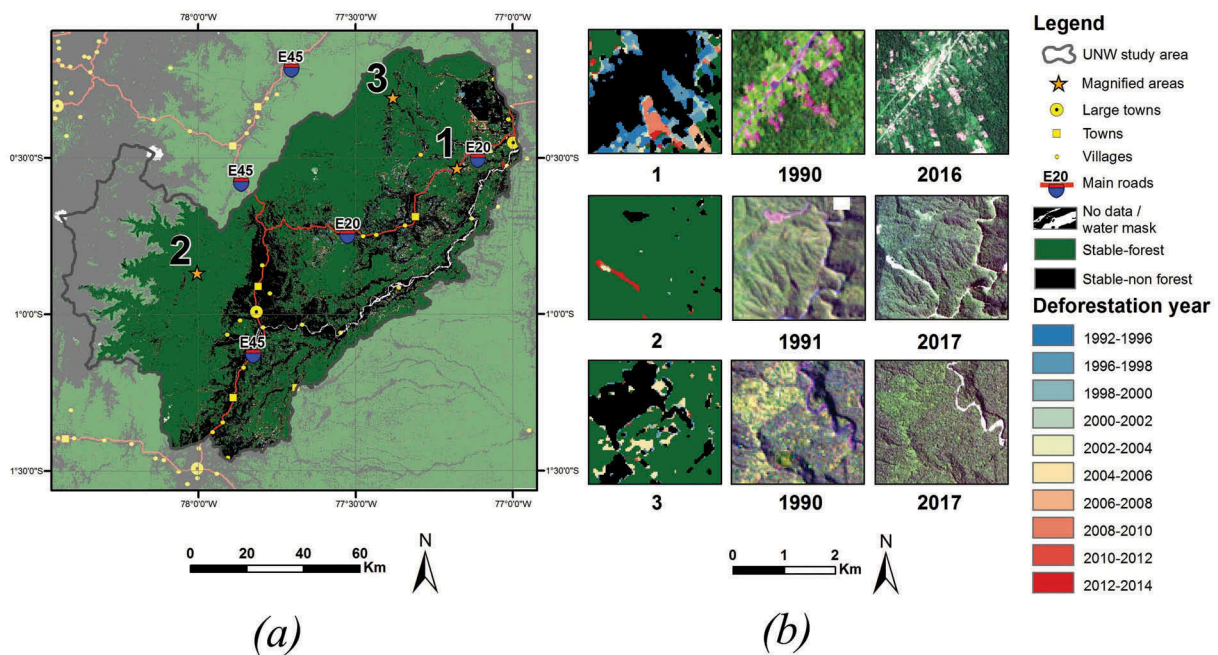| Class name		Deforestation		Reforestation	
		Commission (%)	Omission (%)	Commission (%)	Omission (%)
Stable forest		1	8	5	7
Stable nonforest		11	1	7	5
Change year	1992–1996	14	4	44	7
	1996–1998	20	13	44	3
	1998–2000	20	17	34	20
	2000–2002	16	2	42	19
	2002–2004	30	5	28	22
	2004–2006	26	3	28	10
	2006–2008	28	5	44	12
	2008–2010	20	0	36	9
	2010–2012	24	5	46	10
	2012–2014	24	0	–	–
Overall mean		19.5	5.25	32.54	11.27

Figure 8. (a) Deforestation year map for the UNW. (b) Magnified areas show: (1) linear deforestation along the E45 highway, (2) landslide scars, and (3) false-positive errors in the mixed forest and pasture areas.
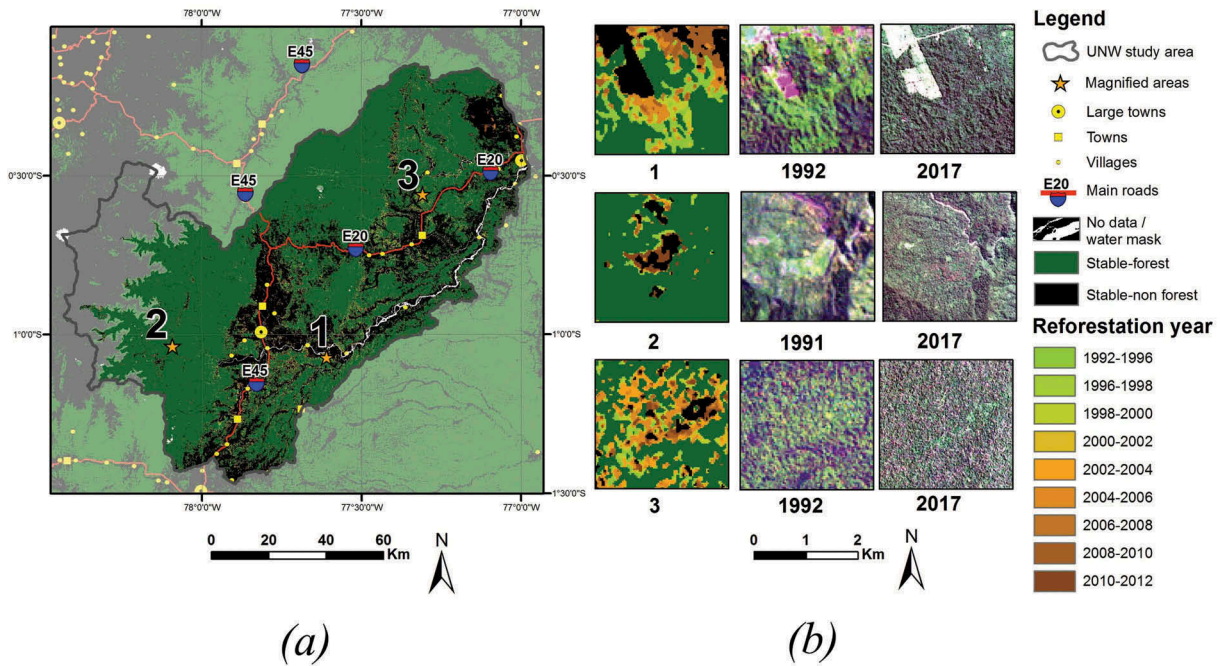
Figure 9. (a) Reforestation year map for the UNW. (b) Magnified areas show: (1) Jatun-Sacha Biological Reserve, which is known for reforestation since the 1990s; (2) forest succession after landslides; and (3) false-positive errors in a stable-forest area.

mask errors than the map of deforestation year (Figure 9(b-3)).

Following Rudel, Bates, and Machinguiashi (2002), we calculated overall deforestation and reforestation by applying a buffer distance of 3 km along the two main highways E45 and E20 in the UNW to corroborate our observations. Accumulated deforestation along highway E45 summed up to an area of 3320 ha and 11,403 ha along highway E20. In contrast, reforestation along highway E45 accumulated to 7458 ha and 5415 ha along highway E20.

Comparison with other sources

We compared our implementation with two different sources: Forest Loss Year (FLY) according to Hansen et al. (2013) and EFR Emission Level information

(MAE, 2017). Both sources were cropped with the UNW and relabeled to match our classes (Figure 10).

Results are similar across the three classifications. However, differences specifically exist with FLY for specific time periods such as 2000–2002 and 2010–2012 (Figure 10(a)) or EFR reforestation between 2008 and 2014 (Figure 10(b)). On average, deforestation was 2757 ha year^{-1} for the period from 2000 to 2014, in FLY data and 4394 ha year^{-1} in EFR. Our estimates are comparably conservative with 2319 ha year^{-1}. According to FAO (Puyravaud, 2003), these values represented annual deforestation rates of −0.35%, −0.57%, and −0.31%, respectively.

Furthermore, reforestation summed up to 574 ha year^{-1} for the 2000–2014 period in FLY, indicated 2277 ha year^{-1} in EFR, and 1504 ha year^{-1} in our analysis, representing annual reforestation rates of
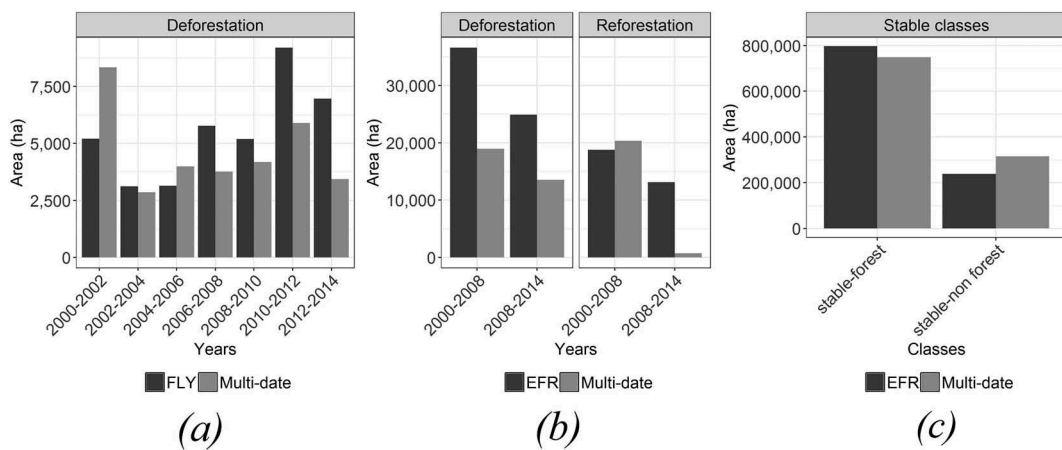
Figure 10. (a) Comparison with FLY by biennials for the period 2000–2014. (b) Comparison with EFR deforestation and reforestation areas for the periods 2000–2008 and 2008–2014, (c) along with unchanged classes.

0.07%, 0.28%, and 0.19%, respectively, in EFR, 796,982 ha stayed unchanged, while our analysis yielded 748,688 ha of stable forests.

Discussion

Biennial image compositing and preprocessing effects on results

Our image compositing technique was based on the standardization and median calculation, which is an effective strategy to maximize information extraction when the number of observations is limited. We chose a biennial classification scheme (Griffiths et al., in review). We thereby improved the signal-to-noise ratio, as 1-year composites may be inferior in data-scarce conditions (Potapov, Turubanova, & Hansen, 2011). Composites from longer time periods, though, may not be adequate to monitor subtle processes such as reforestation (Bustamante et al., 2016).

The histogram matching algorithm that we used for radiometrically aligning the composites enabled a regional-scale classification and at the same time created consistency across the time series. This was supported by the high consistency between the land-cover classifications from different years and the results after applying our postclassification change detection algorithm. However, cloud-free composites as references and sufficient spatial overlap between the target and reference footprints are mandatory for the proper functioning of the histogram matching (Benjamin & Leutner, 2017).

We also accommodated for correcting the radiometric distortions due to topography. In our case, the c-correction algorithm principally improved the homogeneity of the imagery across sunlit and shaded slopes. However, commission errors increased after applying the topography correction. This is in line with the findings in Chance et al. (2016), which reported negative effects of a topographic correction on change detection analysis. Others found that the application of topography correction generally had a smaller influence on the overall accuracy of a classification when compared to the selection of a classifier (Vanonckelen, Lhermitte, & Rompaey, 2015). Future work should further improve the results from topographic correction by employing the best DEMs available (Chance et al., 2016; Pimple et al., 2017).

Postclassification change detection performance

Our postclassification change detection strategy was based on land-cover maps (MAE, 2017) as reference to validate model training and classifier outputs. This allowed the selection of the most precise classifier based on the correlation between the classification and the land-cover maps. While the limited size of our sampling set may not be representative for some classifiers (Zhu et al., 2016), SVMs apparently performed well, as SVMs support small training samples (Wieland, Torres, Pittore, & Benito, 2016).

The original Landsat bands and derived tasseled cap components had a considerable predictive power (Figure 7). This was specifically true for bands 3–7, which are known to be important predictor variables not only in forest/nonforest classifications in the tropics (Potapov et al., 2012) but also in dry regions of the world (Mellor, Haywood, Stone, & Jones, 2013). Spectral mixtures and spectral similarity of land-cover types (see Figure 5(a)) limit the separability at 30-m Landsat spatial resolution. In this regard, elevation and terrain derivatives from the DEM (slope, aspect) contributed to class separation, despite their predictive power not being as high as that of the Landsat bands or tasseled cap components.

While some gaps related to cloud and cloud shadow remnants remained after the classification, we were able to demonstrate that temporal filtering is a powerful technique for removing these artifacts and considerably improving the results (comparison in Table 5). The set of transition rules allowed us to filter most of the illogical class transitions; however, some highly dynamic events were still missed due to the data-scarce setting and accordingly introduced omission errors.

Performance of multi-date classification in the UNW

Despite the remaining limitations of our multi-date classification implementation, the spatially explicit forest dynamics patterns at the UNW allow for novel insights beyond what was already known from previous satellite data analyses relying on only two or just a few points in time (Sierra, 2000) or only spectral information (Walsh, Shao, Mena, & McCleary, 2008) ideally in the Tropical Andes. Dynamics along the E45 highway after 1992 mostly related to reforestation on peripheral lands, while deforestation rates were comparably low in that region (Figure 11(a)).

This may be explained by the population census, where the population in the urban centers of Tena and Archidona increased by 233% between 1990 and 2010 (INEC, 2010), suggesting a rearrangement in the population distribution between the rural and the urban areas. This assumption is supported by similar findings by Rudel et al. (2002) in the Southern Ecuadorian Amazon. In contrast, deforestation was principally identified along the E20 highway. Since this highway was constructed more recently, new settlements and commercial activities linked to oil extraction have triggered deforestation (Wasserstrom & Southgate, 2013; Figure 11(b)).
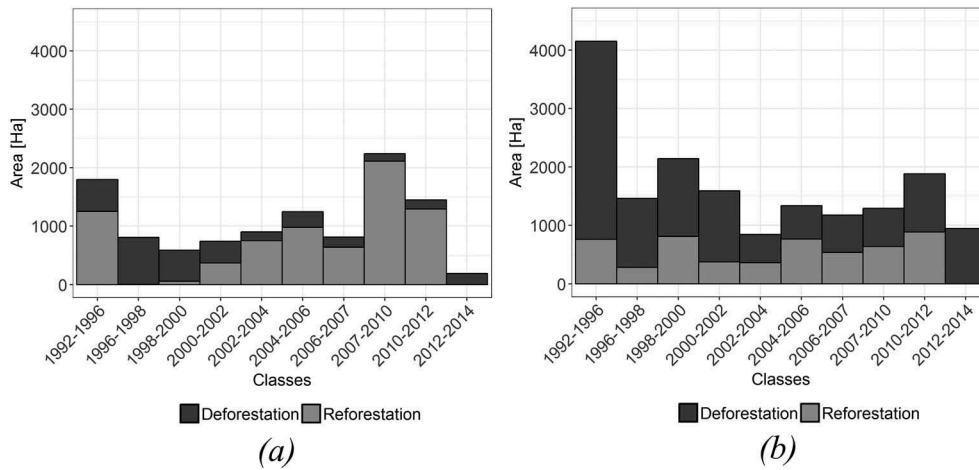
Figure 11. Deforestation/reforestation area for the period 1992–2014 (a) along the highway E45 and (b) along the highway E20.

A comparison with other sources revealed further details. For instance, deforestation showed to be more similar to FLY than to EFR, most likely because the FLY data-set is also based on a multi-date classification, while the EFR was based on an object-based classification that generalized deforestation patches. In the case of reforestation, all results differed markedly. Different conceptualizations of reforestation (Hansen et al., 2013; MAE, 2017) and confusion with secondary forests are likely to be the main reasons. According to Cohen et al. (2017), it is not surprising that forest disturbance maps differ due to semantic and methods differences. Different accuracies and results accordingly relate to multiple factors such as differences in the change detection algorithm, in the quality of specific satellite imagery used, metrics and training information, the time-series density, or the thresholds applied to identify change.

Overall, our multi-date classification implementation was demonstrated to be far less sensitive to data scarcity and atmospheric contamination than other approaches using automated time-series analysis algorithms (Santos et al., 2017).

Conclusions and outlook

Forest dynamics in the complex and vulnerable regions of the Tropical Andes are still under-researched considering remote sensing data analyses (Da Ponte et al., 2015; Oliveras, Anderson, & Malhi, 2014). To the best of our knowledge, this was the first study of its kind that specifically focused on the challenges related to scarce data and the poor signal-to-noise ratio in a long time series for automated forest change analyses in the Tropical Andes. We demonstrated that an adapted implementation of multi-date classification based on image compositing, multi-sensor fusion, and postclassification change detection could mitigate most of these limitations. Our findings add to the expanding body of literature

on such approaches with a focus on data-scarce situations and highlight the importance of the Landsat archive for monitoring decadal land-cover change even in cloudy regions of the world.

Future research should focus on diversifying data sources and predictors as our findings provide further evidence that classification results, specifically when using machine learners, will improve in data-rich environments. Moreover, the increasing web-based availability of high- and very high-resolution data will in the future allow to further improve sample quantity and quality, while semi-automatic approaches (Huang, Weng, Lu, Feng, & Zhang, 2015) and temporal-spectral profiles sampling (Senf, Pflugmacher, Wulder, & Hostert, 2015) are also promising alternatives. Furthermore, since our methodology requires a reforestation time threshold, it would be beneficial considering specific thresholds for different forest communities. This should ideally be based on forest growth models such as FORMIND (Paulick, Dislich, Homeier, Fischer, & Huth, 2017) that support specifying distributions for reforestation time threshold. Additionally, improvements may well be possible with further refined transitioning rules in postclassification filtering or automated solutions with more complex transition rules with an increasing number of land-cover classes (Ahlqvist, 2008; Abercrombie & Friedl, 2016).

As other areas may experience similar or even more severe data scarcity than the UNW, image compositing might be limited to lower observation frequencies. In this regard, regions such as north-central Africa and northern Russia, which have the sparsest Landsat coverage compared to Ecuador (Wulder et al., 2016), may constrain multi-date classification usability to frequencies greater than biennials. Such limitations may, for example, constrain its usability in the frame of reducing emissions from deforestation and forest degradation (REDD+), which requires biennial updates reports for Forest Reference Level Information especially in developing countries (UN-REDD Programme, 2015). Finally,

implementing such a multi-date classification for larger study areas requires cloud-based or high-performance computing (HPC) environments, as the processing is demanding, and it is more effective to "bring the algorithm to the data" than to download massive data-sets. Currently, some alternatives are available (e.g. EODC, 2018; Gorelick et al., 2017; Open Foris, 2015), which allow implementing similar methodologies for large areas. Cloud-based or HPC environments also provide novel opportunities to develop monitoring systems based on sensor constellations, such as Landsat and Sentinel-2 (Wulder et al., 2015).

As optical remote sensing of the core tropics regularly suffers from high cloud cover, integrating newly available imagery will increase change map reliabilities. Linking the vast Landsat archive with the quickly expanding Sentinel-2 archive is, therefore, one of the cornerstones for future improvements (Drusch et al., 2012; Wulder et al., 2016). Such a strategy will also allow to extend the applicability of our approach to larger regions such as the entire Tropical Andes and to ecosystems with more diverse land cover.

Acknowledgments

Author contributions

"F.S. and P.H. conceived the methodology research concept. P.M. conceived the Upper Napo Watershed research concept. F.S. developed and executed the processing. F.S and P.M. performed the fieldwork. F.S. developed the outline and wrote the manuscript. P.H. and P.M. discussed methods and outcomes, and edited the manuscript."

Disclosure statement

No potential conflict of interest was reported by the authors.

Funding

ORCID

Fabián Santos http://orcid.org/0000-0002-8130-4377
Patrick Hostert http://orcid.org/0000-0002-5730-5484

References

Abercrombie, S., & Friedl, M. (2016). Improving the consistency of multitemporal land cover maps using a hidden Markov model. *IEEE Transactions on Geoscience and Remote Sensing*, *54*(2), 703–713. doi:10.1109/TGRS.2015.2463689

Ahlqvist, O. (2008). Extending post-classification change detection using semantic similarity metrics to overcome class heterogeneity: A study of 1992 and 2001 U.S. National Land Cover Database changes. *Remote Sensing of Environment*, *112*(3), 1226–1241. doi:10.1016/j.rse.2007.08.012

Angelsen, A., & Wertz-Kanounnikoff, S. (2008). *Realising REDD+: National strategy and policy options. Realising REDD+: National strategy and policy options*. https://doi.org/361

Armenteras, D., María, J., Rodríguez, N., & Retana, J. (2017). Deforestation dynamics and drivers in different forest types in Latin America : Three decades of studies (1980 – 2010). *Global Environmental Change*, *46*(June), 139–147. doi:10.1016/j.gloenvcha.2017.09.002

Armenteras, D., Rodríguez, N., Retana, J., & Morales, M. (2011). Understanding deforestation in montane and lowland forests of the Colombian Andes. *Regional Environmental Change*, *11*(3), 693–705. doi:10.1007/s10113-010-0200-y

Arvidson, T., Gasch, J., & Goward, S.N. (2001). Landsat 7's long-term acquisition plan – an innovative approach to building a global imagery archive. *Remote Sensing of Environment*, *78*(1–2), 13–26. doi:10.1016/S0034-4257(01)00263-2

Asner, G.P., Anderson, C.B., Martin, R.E., Knapp, D.E., Tupayachi, R., Sinca, F., & Malhi, Y. (2014). Landscape-scale changes in forest structure and functional traits along an Andes-to-Amazon elevation gradient. *Biogeosciences*, *11*(3), 843–856. doi:10.5194/bg-11-843-2014

Barbosa, J.M., Broadbent, E.N., & Bitencourt, M.D. (2014). Remote sensing of aboveground biomass in tropical secondary forests: A review. *International Journal of Forestry Research*, 1–14. doi:10.1155/2014/715796

Bengtsson, H. (2016). matrixStats: Functions that Apply to Rows and Columns of Matrices (and to Vectors), Version 0.50.2. Retrieved from https://cran.r-project.org/package=matrixStats

Benjamin, A., & Leutner, M.B. (2017). RStoolbox: Toolbox for remote sensing image processing and analysis such as calculating spectral indices, principal component transformation, unsupervised and supervised classification or fractional cover analyses, Version 0.1.9. Retrieved from https://github.com/bleutner/RStoolbox

Brown, S., & Lugo, A. (1990). Tropical secondary forests. *Journal of Tropical Ecology*, Cambridge University Press. doi:10.1017/S0266467400003989

Bustamante, M.M.C., Roitman, I., Aide, T.M., Alencar, A., Anderson, L.O., Aragão, L., … Vieira, I.C.G. (2016). Toward an integrated monitoring framework to assess the effects of tropical forest degradation and recovery on carbon stocks and biodiversity. *Global Change Biology*, *22*(1), 92–109. doi:10.1111/gcb.13087

Camara, G. (2013). *Programa Amazônia – Projeto PRODES*. Instituto Nacional de Pesquisas Espaciais, São Jose dos Campos..

CGIAR – CSI. (2008). SRTM 90m DEM, Version 4. Retrieved from http://srtm.csi.cgiar.org/index.asp

Chance, C.M., Hermosilla, T., Coops, N.C., Wulder, M.A., & White, J.C. (2016). Effect of topographic correction on forest change detection using spectral trend analysis of Landsat pixel-based composites. *International Journal of Applied Earth Observation and Geoinformation*, *44*, 186–194. doi:10.1016/j.jag.2015.09.003

Clark, M.L., Aide, T.M., Grau, H.R., & Riner, G. (2010). A scalable approach to mapping annual land cover at 250 m using MODIS time series data: A case study in the Dry Chaco ecoregion of South America. *Remote Sensing of Environment*, *114*(11), 2816–2832. doi:10.1016/j.rse.2010.07.001

Clayden, J. (2016). mmand: Mathematical Morphology in Any Number of Dimensions, Version 1.4.0. Retrieved from https://cran.r-project.org/package=mmand

Cohen, W.B., Healey, S.P., Yang, Z., Stehman, S.V., Brewer, C.K., Brooks, E.B., … Zhu, Z. (2017). How similar are forest disturbance maps derived from different landsat time series algorithms? *Forests*, *8*(4), 1–19. doi:10.3390/f8040098

Congalton, R.G. (1991). A review of assessing the accuracy of classifications of remotely sensed data. *Remote Sensing of Environment*, *37*(1), 35–46. doi:10.1016/0034-4257(91)90048-B

Crist, E. P., & Cicone, R. C. (1984). A physically-based transformation of thematic mapper data-the tm tasseled cap. *Ieee Transactions on Geoscience and Remote Sensing*, *GE-22(3)*, 256–263. doi:10.1109/TGRS.1984.350619

Da Ponte, E., Fleckenstein, M., Leinenkugel, P., Parker, A., Oppelt, N., & Kuenzer, C. (2015). Tropical forest cover dynamics for Latin America using Earth observation data: A review covering the continental, regional, and local scale. *International Journal of Remote Sensing*, *36* (12), 3196–3242. doi:10.1080/01431161.2015.1058539

De Fries, R.S., Hansen, M.C., Townshend, J.R.G., & Sohlberg, R. (1998). Global land cover classifications at 8 km spatial resolution: The use of training data derived from Landsat imagery in decision tree classifiers. *International Journal of Remote Sensing*, *19*(16), 3141–3168. doi:10.1080/014311698214235

De Koning, F., Aguinaga, M., Bravo, M., Chiu, M., Lascano, M., Lozada, T., & Suarez, L. (2011). Bridging the gap between forest conservation and poverty alleviation: The Ecuadorian Socio Bosque program. *Environmental Science and Policy*, *14* (5), 531–542. doi:10.1016/j.envsci.2011.04.007

Drusch, M., Del Bello, U., Carlier, S., Colin, O., Fernandez, V., Gascon, F., … Bargellini, P. (2012). Sentinel-2: ESA's optical high-resolution mission for GMES operational services. *Remote Sensing of Environment*, *120*, 25–36. doi:10.1016/j.rse.2011.11.026

Edwards, D.P., Massam, M.R., Haugaasen, T., & Gilroy, J.J. (2017). Tropical secondary forest regeneration conserves high levels of avian phylogenetic diversity. *Biological Conservation*, *209*, 432–439. doi:10.1016/j.biocon.2017.03.006

Eklundh, L., & Jönsson, P. (2015). *TIMESAT: A software package for time-series processing and assessment of vegetation dynamics.* (Vol. 22), 141–158Springer International Publishing, Retrieved from. Doi: 10.1007/978-3-319-15967-6_7

EODC. (2018). Earth observation data centre for water resources monitoring: An open and international cooperation to foster the use of earth observation data. Retrieved May 18, 2018, from https://www.eodc.eu/

Espinoza, J.C., Chavez, S., Ronchail, J., Junquas, C., Takahashi, K., & Lavado, W. (2015). Rainfall hotspots over the southern tropical Andes: Spatial distribution, rainfall intensity, and relations with large-scale atmospheric circulation. *Water Resources Research*, *51*(5), 3459–3475. doi:10.1002/2014WR016273

Fearnside, P.M. (2005). Deforestation in Brazilian Amazonia: History, rates, and consequences. *Conservation Biology*, *19* (3), 680–688. doi:10.1111/cbi.2005.19.issue-3

Fragal, E.H., Silva, T.S.F., & Novo, E.M.L.D.M. (2016). Reconstructing historical forest cover change in the Lower Amazon floodplains using the LandTrendr algorithm. *Acta Amazonica*, *46*(1), 13–24. doi:10.1590/1809-4392201500835

GDAL Development Team. (2017). GDAL – Geospatial Data Abstraction Library, Version 2.0.1. Retrieved from http://www.gdal.org

Gorelick, N., Hancher, M., Dixon, M., Ilyushchenko, S., Thau, D., & Moore, R. (2017). Google Earth Engine: Planetary-scale geospatial analysis for everyone. *Remote Sensing of Environment*. doi:10.1016/j.rse.2017.06.031

Griffiths, P., Kuemmerle, T., Baumann, M., Radeloff, V.C., Abrudan, I.V., Lieskovsky, J., … Hostert, P. (2014). Forest disturbances, forest recovery, and changes in forest types across the carpathian ecoregion from 1985 to 2010 based on landsat image composites. *Remote Sensing of Environment*, *151*, 72–88. doi:10.1016/j.rse.2013.04.022

Guariguata, M.R., & Ostertag, R. (2001). Neotropical secondary forest succession: Changes in structural and functional characteristics. *Forest Ecology and Management*, *148*(1–3), 185–206. doi:10.1016/S0378-1127(00)00535-1

Hansen, M.C., & Loveland, T.R. (2012). A review of large area monitoring of land cover change using Landsat data. *Remote Sensing of Environment*, *122*, 66–74. doi:10.1016/j.rse.2011.08.024

Hansen, M.C., Potapov, P., Moore, R., Hancher, M., Turubanova, S., Tyukavina, A., … Townshend, J.R.G. (2013). High-resolution global maps of 21st-century forest cover change. *Science*, *342*(6160), 850–853. doi:10.1126/science.1244693

Hansen, M.C., Roy, D., Lindquist, E., Adusei, B., Justice, C., & Altstatt, A. (2008). A method for integrating MODIS and Landsat data for systematic monitoring of forest cover and change in the Congo Basin. *Remote Sensing of Environment*, *112*(5), 2495–2513. doi:10.1016/j.rse.2007.11.012

Hijmans, R. (2016). raster: Geographic data analysis and modeling. Retrieved from https://cran.r-project.org/package=raster

Hoorn, C., Wesselingh, F.P., Ter Steege, H., Bermudez, M.A., Mora, A., Sevink, J., … Antonelli, A. (2010). Amazonia through time: Andean uplift, climate change, landscape evolution, and biodiversity. *Science*, *330* (November), 927–931. doi:10.1126/science.1194585

Huang, X., Weng, C., Lu, Q., Feng, T., & Zhang, L. (2015). Automatic labelling and selection of training samples for high-resolution remote sensing image classification over urban areas. *Remote Sensing*, *7*(12), 16024–16044. doi:10.3390/rs71215819

INEC. (2010). Censo de Población y Vivienda 2010. Instituto Nacional de Estadísticas y Censos. Retrieved from http://www.inec.gob.ec/estadisticas/

Karatzoglou, A., Smola, A., Hornik, K., & Zeileis, A. (2004). kernlab – An S4 package for kernel methods in R. Journal of Statistical Software, 11(9), 1–20. doi:10.18637/jss.v011.i09

Karmalkar, A.V., Bradley, R.S., & Diaz, H.F. (2008). Climate change scenario for Costa Rican montane forests. Geophysical Research Letters, 35(11), 1–5. doi:10.1029/2008GL033940

Karnieli, A., Kaufman, Y. J., Remer, L., & Wald, A. (2001). Afri - aerosol free vegetation index. Remote Sensing Of Environment, 77(1),10–21. doi:10.1016/S0034-4257(01)00190-0

Kennedy, R.E., Yang, Z., & Cohen, W.B. (2010). Detecting trends in forest disturbance and recovery using yearly Landsat time series: 1. LandTrendr – Temporal segmentation algorithms. Remote Sensing of Environment, 114(12), 2897–2910. doi:10.1016/j.rse.2010.07.008

Key, C. H., & Benson, N. C. (2006). Landscape Assessment: Ground measure of severity, the Composite Burn Index; and Remote sensing of severity, the Normalized Burn Ratio. Ogden, UT: USDA Forest Service, Rocky Mountain Research Station.

Kimes, D.S., Nelson, R.F., Skole, D.L., & Salas, W.A. (1998). Accuracies in mapping secondary tropical forest age from sequential satellite imagery. Remote Sensing of Environment, 65(1), 112–120. doi:10.1016/S0034-4257(98)00021-2

Krishna Bahadur, K. C. (2009). Improving landsat and irs image classification: evaluation of unsupervised and supervised classification through band ratios and dem in a mountainous landscape in nepal. Remote Sensing, 1(4),1257–1272. doi:10.3390/rs1041257

Kuemmerle, T., Erb, K., Meyfroidt, P., Müller, D., Verburg, P.H., Estel, S., … Reenberg, A. (2013). Challenges and opportunities in mapping land use intensity globally. Current Opinion in Environmental Sustainability, 5(5), 484–493. doi:10.1016/j.cosust.2013.06.002

Kuhn, M. (2016). caret: Classification and Regression Training, Version 6.0-71. Retrieved from https://cran.r-project.org/package=caret

Lunetta, R., Johnson, J., Lyon, G., & Crotwell, J. (2004). Impacts of imagery temporal frequency on land-cover change detection monitoring. In Remote Sensing of Environment Environment (pp. 444–454).

MAE. (2013). Metodología para la representación Cartográfica de los Ecosistemas del Ecuador Continental. S. de Patrimonio Natural. Ed., Author.

MAE. (2017). Documentation of the information used for the establishment of Ecuador's forest reference emission level. Retrieved August 16, 2017, from http://suia.ambiente.gob.ec/web/suia/anexos-nivel-referencia

Masek, J.G., Vermote, E.F., Saleous, N., Wolfe, R., Hall, F.G., Huemmrich, F., & Gao, J.K. (2012). LEDAPS calibration, reflectance, atmospheric correction preprocessing code, version 2. Model product. Computer program, Oak Ridge. Tennessee, U.S.A: Oak Ridge National Laboratory Distributed Active Archive Center.

Mellor, A., Haywood, A., Stone, C., & Jones, S. (2013). The performance of random forests in an operational setting for large area sclerophyll forest classification. Remote Sensing, 5(6), 2838–2856. doi:10.3390/rs5062838

Müller, H., Griffiths, P., & Hostert, P. (2016). Long-term deforestation dynamics in the Brazilian Amazon — Uncovering historic frontier development along the Cuiabá – Santarém highway. International Journal of Applied Earth Observations and Geoinformation, 44, 61–69. doi:10.1016/j.jag.2015.07.005

NASA. (2011). Landsat 7 science data users handbook. National Aeronautics and Space Administration (NASA). Retrieved from https://landsat.gsfc.nasa.gov

National Institute of Advanced Industrial Science and Technology, & Geological Survey Japan. (2017). MADAS: METI AIST satellite data archive system. Retrieved August 16, 2017, from https://gbank.gsj.jp/

Oliveira, R.S., Eller, C.B., Bittencourt, P.R.L., & Mulligan, M. (2014). The hydroclimatic and ecophysiological basis of cloud forest distributions under current and projected climates. Annals of Botany, 113(6), 909–920. doi:10.1093/aob/mcu060

Oliveras, I., Anderson, L.O., & Malhi, Y.S. (2014). Application of remote sensing to understanding fire regime and biomass burning emissions of the tropical Andes. Global Biogeochemical Cycles, 28, 480–496. doi:10.1002/2013GB004664.Received

Olofsson, P., Foody, G.M., Herold, M., Stehman, S.V., Woodcock, C.E., & Wulder, M.A. (2014). Good practices for estimating area and assessing accuracy of land change. Remote Sensing of Environment, 148, 42–57. doi:10.1016/j.rse.2014.02.015

Open Foris. (2015). System for earth observations, data access, processing & analysis for land monitoring (SEPAL). Retrieved from https://sepal.io/

Paula, F.S., Rodrigues, J.L.M., Zhou, J., Wu, L., Mueller, R.C., Mirza, B.S., … Pellizari, V.H. (2014). Land use change alters functional gene diversity, composition and abundance in Amazon forest soil microbial communities. Molecular Ecology, 23(12), 2988–2999. doi:10.1111/mec.12786

Paulick, S., Dislich, C., Homeier, J., Fischer, R., & Huth, A. (2017). The carbon fluxes in different successional stages: Modelling the dynamics of tropical montane forests in South Ecuador. Forest Ecosystems, 4(1), 5. doi:10.1186/s40663-017-0092-0

Pflugmacher, D., Cohen, W.B., & Kennedy, R.E. (2012). Using Landsat-derived disturbance history (1972–2010) to predict current forest structure. Remote Sensing of Environment, 122, 146–165. doi:10.1016/j.rse.2011.09.025

Pimple, U., Sitthi, A., Simonetti, D., Pungkul, S., Leadprathom, K., & Chidthaisong, A. (2017). Topographic correction of Landsat TM-5 and Landsat OLI-8 imagery to improve the performance of forest classification in the mountainous terrain of Northeast Thailand. Sustainability (Switzerland), 9(2), 1–26. doi:10.3390/su9020258

Poorter, L., Bongers, F., Aide, T.M., Almeyda Zambrano, A.M., Balvanera, P., Becknell, J.M., … Rozendaal, D.M.A. (2016). Biomass resilience of Neotropical secondary forests. Nature, 530(7589), 211–214. doi:10.1038/nature16512

Potapov, P., Turubanova, S., & Hansen, M.C. (2011). Regional-scale boreal forest cover and change mapping using Landsat data composites for European Russia. Remote Sensing of Environment, 115(2), 548–561. doi:10.1016/j.rse.2010.10.001

Potapov, P.V., Turubanova, S.A., Hansen, M.C., Adusei, B., Broich, M., Altstatt, A., … Justice, C.O. (2012). Quantifying forest cover loss in Democratic Republic of the Congo, 2000–2010, with Landsat ETM+ data. Remote Sensing of Environment, 122, 106–116. doi:10.1016/j.rse.2011.08.027

Pueschel, P., Buddenbaum, H., & Hill, J. (2012). An efficient approach to standardizing the processing of hemispherical images for the estimation of forest structural attributes. Agricultural and Forest Meteorology, 160, 1–13. doi:10.1016/j.agrformet.2012.02.007

Puyravaud, J.P. (2003). Standardizing the calculation of the annual rate of deforestation. Forest Ecology and Management, 177(1–3), 593–596. doi:10.1016/S0378-1127(02)00335-3

R Development Core Team. (2017). The R project for statistical computing, version 3.4.3. GNU project. Retrieved from http://www.r-project.org/

RAISG. (2015). *Deforestation in the Amazonia (1970–2013)*. Retrieved from www.raisg.socioambiental.org

Ramírez, B., Teuling, A.J., Ganzeveld, L., Hegger, Z., & Leemans, R. (2017). Tropical montane cloud forests: Hydrometeorological variability in three neighbouring catchments with different forest cover. *Journal of Hydrology*, 552, 151–167. doi:10.1016/j.jhydrol.2017.06.023

Riaño, D., Chuvieco, E., Salas, J., & Aguado, I. (2003). Assessment of different topographic corrections in land-sat-TM data for mapping vegetation types. *IEEE Transactions on Geoscience and Remote Sensing*, 41 (5PART 1), 1056–1061. doi:10.1109/TGRS.2003.811693

Rouse, J., Haas, R. H., Scheel, J. A., & Deering, D. W. (1974). Monitoring vegetation systems in the great plains with erts. In Proceedings, 3rd Earth Resource Technology Satellite (ERTS) Symposium (Vol. *1*, pp. 48–62).

Rudel, T.K., Bates, D., & Machinguiashi, R. (2002). A tropical forest transition? Agricultural change, out-migration, and secondary forests in the Ecuadorian Amazon. *Annals of the Association of American Geographers*, 92(1), 87–102. doi:10.1111/1467-8306.00281

Rufin, P., Müller, H., Pflugmacher, D., & Hostert, P. (2015). Land use intensity trajectories on Amazonian pastures derived from Landsat time series. *International Journal of Applied Earth Observation and Geoinformation*, 41, 1–10. doi:10.1016/j.jag.2015.04.010

Santos, F., Dubovyk, O., & Menz, G. (2017). Monitoring forest dynamics in the Andean Amazon: The applicability of breakpoint detection methods using landsat time-series and genetic algorithms. *Remote Sensing*, 9, 1. doi:10.3390/rs9010068

Senf, C., Pflugmacher, D., Wulder, M.A., & Hostert, P. (2015). Characterizing spectral-temporal patterns of defoliator and bark beetle disturbances using Landsat time series. *Remote Sensing of Environment*, 170, 166–177. doi:10.1016/j.rse.2015.09.019

Sierra, R. (2000). Dynamics and patterns of deforestation in the western Amazon: The Napo deforestation front, 1986–1996. *Applied Geography*, 20(1), 1–16. doi:10.1016/S0143-6228(99)00014-4

Silman, M.R., Ancaya, E.J., & Brinson, J. (2003). Los bosques de bambú en la amazonía occidental. In R. Leite, N. Pitman, & P. Álvarez (Eds.), *Alto Purús: Biodiversidad, Conservación y Manejo* (pp. 62–73).

Spracklen, D.V., & Righelato, R. (2014). Tropical montane forests are a larger than expected global carbon store. *Biogeosciences*, 11(10), 2741–2754. doi:10.5194/bg-11-2741-2014

Thomas, N.E., Huang, C., Goward, S.N., Powell, S., Rishmawi, K., Schleeweis, K., & Hinds, A. (2011). Validation of North American Forest disturbance dynamics derived from Landsat time series stacks. *Remote Sensing of Environment*, 115(1), 19–32. doi:10.1016/j.rse.2010.07.009

UN-REDD Programme. (2015). Technical considerations for forest reference emission level and/or forest reference level construction for REDD+ under the UNFCCC, 31. Retrieved from http://www.unredd.net/index.php?option=com_docman&view=document&alias=14118-technical-considerations-for-forest-reference-emission-level-andor-forest-reference-level-construction-for-redd-under-the-unfccc&category_slug=frl&Itemid=134

USGS. (2014). Earth resources observation and science (EROS) center science processing architecture (ESPA) on demand interface. Retrieved January 14, 2017, from https://espa.cr.usgs.gov

Vanonckelen, S., Lhermitte, S., & Rompaey, A.V. (2015). The effect of atmospheric and topographic correction on pixel-basedimage composites: Improved forest cover detection in mountainenvironments. *International Journal of Applied Earth Observation and Geoinformation*, 35(PB), 320–328. doi:10.1016/j.jag.2014.10.006

Verbesselt, J., Hyndman, R., Newnham, G., & Culvenor, D. (2010). Detecting trend and seasonal changes in satellite image time series. *Remote Sensing of Environment*, 114 (1), 106–115. doi:10.1016/j.rse.2009.08.014

Walsh, S.J., Shao, Y., Mena, C.F., & McCleary, A.L. (2008). Integration of hyperion satellite data and household social survey to characterize the causes and consequences of reforestation patterns in the northern Ecuadorian Amazon. *Photogrammetric Engineering & Remote Sensing*, 74(6), 725–735. doi:10.14358/PERS.74.6.725

Wasserstrom, R., & Southgate, D. (2013). Deforestation, agrarian reform and oil development in Ecuador, 1964–1994. *Natural Resources*, 04(01), 31–44. doi:10.4236/nr.2013.41004

Revolution Analytics, & Weston, S. (2015). foreach: Provides Foreach Looping Construct for R, Version 1.4.3. Retrieved from https://cran.r-project.org/package=foreach

Wieland, M., Torres, Y., Pittore, M., & Benito, B. (2016). Object-based urban structure type pattern recognition from Landsat TM with a support vector machine. *International Journal of Remote Sensing*, 37(17), 4059–4083. doi:10.1080/01431161.2016.1207261

Wilson, M.F.J., O'Connell, B., Brown, C., Guinan, J.C., & Grehan, A.J. (2007). Multiscale terrain analysis of multibeam bathymetry data for habitat mapping on the continental slope. *Marine Geodesy*, 30. doi:10.1080/01490410701295962

Wulder, M.A., Hilker, T., White, J.C., Coops, N.C., Masek, J.G., Pflugmacher, D., & Crevier, Y. (2015). Virtual constellations for global terrestrial monitoring. *Remote Sensing of Environment*, 170, 62–76. doi:10.1016/j.rse.2015.09.001

Wulder, M.A., White, J.C., Loveland, T.R., Woodcock, C.E., Belward, A.S., Cohen, W.B., ... Roy, D.P. (2016). The global Landsat archive: Status, consolidation, and direction. *Remote Sensing of Environment*, 185, 271–283. doi:10.1016/j.rse.2015.11.032

Zhang, M., Carder, K., Muller-Karger, F.E., Lee, Z., & Goldgof, D.B. (1999). Noise reduction and atmospheric correction for coastal applications of Landsat thematic mapper imagery. *Remote Sensing of Environment*, 70(2), 167–180. doi:10.1016/S0034-4257(99)00031-0

Zhu, Z. (2017). Change detection using Landsat time series: A review of frequencies, preprocessing, algorithms, and applications. *ISPRS Journal of Photogrammetry and Remote Sensing*, 130, 370–384. doi:10.1016/j.isprsjprs.2017.06.013

Zhu, Z., Gallant, A.L., Woodcock, C.E., Pengra, B., Olofsson, P., Loveland, T.R., ... Auch, R.F. (2016). Optimizing selection of training and auxiliary data for operational land cover classification for the LCMAP initiative. *ISPRS Journal of Photogrammetry and Remote Sensing*, 122, 206–221. doi:10.1016/j.isprsjprs.2016.11.004

Zhu, Z., & Woodcock, C.E. (2012). Object-based cloud and cloud shadow detection in Landsat imagery. *Remote Sensing of Environment*, 118, 83–94. doi:10.1016/j.rse.2011.10.028

Zhu, Z., & Woodcock, C.E. (2014). Continuous change detection and classification of land cover using all available Landsat data. *Remote Sensing of Environment*, 144, 152–171. doi:10.1016/j.rse.2014.01.011